UNIVERSITY OF CALIFORNIA SAN DIEGO

Wave-Slope Soaring of the Brown Pelican

A Thesis submitted in partial satisfaction of the requirements for the degree

Master of Science

in

Mechanical and Aerospace Engineering

by

Ian Alexander Stokes

Committee in charge:

Professor Andrew Lucas, Chair
Professor Stefan Llewellyn-Smith, Co-Chair
Professor David Saintillan

2019

The Thesis of Ian Stokes is approved, and it is acceptable in quality and form for publication on microfilm and electronically:

Co-Chair

Chair

University of California San Diego

2019

Table of Contents

List of Figures

List of Tables

ABSTRACT OF THE THESIS

Wave-Slope Soaring of the Brown Pelican

by

Ian Alexander Stokes

Master of Science in Mechanical and Aerospace Engineering

University of California San Diego, 2019

Professor Andrew Lucas, Chair
Professor Stefan Llewellyn-Smith, Co-Chair

We theoretically assess the energy savings associated with wave-slope soaring of the brown pelican over near-shoaling ocean surface waves. The steady, constant altitude flight of a pelican is analyzed as a control. The airflow induced by a passing wave, or the "wave-induced wind," is theoretically analyzed for shallow water solitary waves. These waves are assumed to be well described by the KdV equation. We use potential flow theory to describe the wave-induced wind. Using a regular expansion of the Stokes stream function and the Green's function for Laplace in 2D with Dirichlet boundary conditions, we obtain integral expressions for the horizontal and vertical components of the wave-induced wind in a frame of reference moving with the wave. The theory results in expressions wherein provided with the amplitude and period of an incoming swell, horizontal and vertical components of the wave-induced wind in a frame of reference moving with the wave are produced. Wave-slope soaring flight is analyzed over near-shoaling solitary waves on size scales corresponding to wind swell, with amplitude of 1m and period of 10s. We find an upper bound benefit of 57.6% decrease in required mechanical power output as compared with flight out of ground effect and 52.4% benefit as compared with standard ground effect flight. The theory in this work define sufficient evidence that wave-slope soaring could become a viable strategy for energy efficient flight of unmanned autonomous vehicles (UAVs).

Introduction

We theoretically assess the energy savings associated with wave-slope soaring flight. In particular, we study the brown pelican practicing wave-slope soaring over near-shoaling, coastal, ocean surface waves. Wave slope soaring is a common practice of seabirds whereby updrafts resulting from near-shoaling waves are utilized in combination with ground effect to achieve energy efficient flight. Some birds, such as cormorants, flap throughout this process while others, such as the brown pelican, soar through these updrafts. This paper will focus on soaring flight as opposed to flapping flight.

Studies of the various means of soaring used by birds have gained attention in industry due to their practical application to programming unmanned autonomous vehicles (UAVs). Albatrosses have received significant attention with their practice of "dynamic soaring." Dynamic soaring has been a topic of research for decades and remains active, particularly for biomimicry by UAVs. The dynamic soaring process has been detailed by Wilson (1975), formalized by Denny (2009), and experimentally verified by Sachs (2013), to name a few of those who have studied this flight mechanism. In short, the birds use the shear layer above the ocean on windy days to accelerate and soar for extended periods of time without flapping. The mechanism is comparable to the tacking of a sailboat in order to make way upwind.

Richardson (2011) studied the conditions wherein dynamic soaring becomes a cost-effective method of flight. It was found that when the winds are strong, dynamic soaring was preferred, regardless of sea surface conditions. When the winds are light, but surface conditions provide swell, wave-slope soaring becomes the albatross' dominant method of travel. In conditions of light wind and minimal surf, rather than flight via flapping, albatrosses simply sit on the ocean surface until the wind or waves return. As the albatrosses are reluctant to fly without using either dynamic or wave-slope soaring flight, it seems clear that there must be significant benefit to both of these means of flight. While dynamic soaring has been widely studied, wave-slope soaring has not received much attention in the literature. There is no proper formalism regarding wave-slope soaring, and it has rarely been mentioned outside of the study by Richardson (2011). In this paper we aim to create a theoretical formalism from which experimental research as well as application for UAV mimicry can stem.

Chapter 1

Pelican Flight in Absence of Ocean Waves

1.1 Assumptions and Parameters

First off, we will make some assumptions about the nature of the air flow over a brown pelican's wings. The dynamic viscosity of air is small ($\mu \approx 1.8 * 10^{-5}\ \frac{\text{N}\cdot\text{s}}{\text{m}} \ll 1$) over the relevant temperature range, thus (1) we assume inviscid flow. The Mach number can be expressed as $\text{Ma} = u_c/c$ where c is the speed of sound. As we model the flow of the air over the pelicans wings, $c \to c_{air} \approx 343$ m/s. Pennycuick (1982), through observational studies, determined the average speed of a brown pelican in straight flight to be roughly 10 m/s, which we will use as the characteristic velocity u_c for Mach and Reynolds number analyses. Plugging into the relation for Ma we see that ($\text{Ma} \approx 10/343 \approx 0.03$) is much less than the critical Mach number ($\text{Ma}_c = 0.2$). Consequently, (2) we may ignore compressible effects in this flow. The air above the ocean typically does not exhibit large changes of density over the length scales of soaring flight, thus (3) assume the density of air (ρ) to be constant throughout the flow.

As the flow is now assumed to be inviscid and exists within an incompressible fluid of constant density, it is appropriate to (4) assume that the air flowing over the pelican's wing will act as an ideal fluid and the flow will be governed by Euler's equations. As the flow in the bird's frame of reference is ideal and also irrotational, we can look at the cross section of a pelican wing and use potential flow theory to analyze the flow. This allows us to use the Kutta-Joukowski

Table 1.1: Average Brown Pelican Parameters, as given by Pennycuick (1982).

Mass	M	2.65 kg
Wingspan	b	2.10 m
Total Wing Area	S	0.45 m^2
Wing Loading	W/S	57.8 N/m^2
Aspect Ratio	A	9.8

theorem to discuss lift and drag experienced by the bird. From observation, the angle of attack of pelican soaring flight is sufficiently small, as these birds do not tend to stall. Therefore (5) we use the small angle approximation to set the planform area (A_p) equal to the full area of the wing (S). Furthermore, the small angle of attack and low Mach number allows us to assume that (6) to first approximation flow separation will not occur.

Pennycuick (1982) used the study of elliptic wing loading to obtain the lift coefficient of the Brown Pelican in straight flight out of ground effect. (7) Elliptic loading is a reasonable approximation for the shape of the pelican represented as an airfoil, as viewed from above or below. The value of coefficient of lift was experimentally determined by Pennycuick (1982) as $C_L = 0.72$. Pennycuick (1982) also took measurements of various average brown pelican parameters, given in table 1.1. In a later study, Pennycuick et al (1987) deliver an experimentally derived relation for determining the body drag coefficients of large waterfowl and raptors, C_D, as a function of Reynolds number. This relation is given

$$\forall \, \mathrm{Re} \in (5 * 10^5, 2 * 10^6) \implies C_D \approx 1.57 - 0.108 \ln(\mathrm{Re}). \tag{1.1}$$

Using characteristic velocity and length scales corresponding to the flow over a pelican's wing, we can assess the associated Reynolds number. The relevant characteristic length and velocity scales are the average chord length of a pelican's wing and the average speed of slope-soaring flight, respectively. Martin (2017) took a 3D scan of a Brown Pelican wing and recorded a sectional dataset of various wing properties. From this table we find the average chord length ($\bar{c}$) of the particular pelican wing that Martin (2017) studied to be $\bar{c} \approx 0.233$ m. As a sanity check, we calculate the standard mean chord (SMC) assuming a straight tapered wing using the average pelican measurements given by Pennycuick (1982). This calculation yields

$$SMC = \frac{S}{b} = 0.21 \text{ m}. \tag{1.2}$$

With this quick check we find close agreement with the average chord derived from the 3D scan. The study by Martin (2017) deals with one particular pelican and therefore we may not assume this result accurately reflects the entire population. Measurements given by Pennycuick (1982) however, were taken from a sufficiently large dataset such that the average values given do represent the population reasonably well, thus we will continue using $\bar{c} = 0.21$ m. Carrying on with these characteristic values as well as the density and viscosity of air at room temperature, we obtain the Reynolds number as

$$\mathrm{Re} = \frac{l_c u_c \rho}{\mu} \approx 150,000. \tag{1.3}$$

Our calculated Reynolds number lies between 50,000 and 200,000, and consequently we may determine the approximate body drag coefficient using the relation given by Pennycuick et al (1987) yielding

$$C_D = 1.57 - 0.108 \ln(150,000) \approx 0.28. \tag{1.4}$$

This value falls within the predicted range for large waterfowl, $C_D \in (0.20, 0.40)$, as given by Pennycuick et al (1987).

1.2 Flight out of Ground Effect

In order to analyze cost benefits of flight in ground effect, we must first obtain a baseline comparison through analysis of the steady, constant altitude flight of a pelican in still air, out of ground effect. Throughout this section we will use a standard force balance approach. We will define a coordinate system such that $\hat{\mathbf{z}}$ represents the vertical unit vector and $\hat{\mathbf{x}}$ represents the horizontal unit vector. Furthermore, we will follow the lifting line theory of flight in ground effect with a fixed wing detailed by Rayner (1991). Starting with the Kutta-Joukowski theorem we obtain an expression for the total lift ($\mathbf{L}$) across full wingspan in terms of air density (ρ), wingspan (b), wing root circulation (Γ_0), and overwing airspeed in pelican's frame of reference (u) as

$$\mathbf{L} = \frac{\pi \rho b u \Gamma_0}{4} \hat{\mathbf{z}}. \tag{1.5}$$

From the balance of lift and weight ($\mathbf{L} = Mg\hat{\mathbf{z}}$) which is required for steady, level flight, we derive an expression for the wing root circulation Γ_0 as a function of u yielding

$$\Gamma_0(u) = \frac{4Mg}{\pi\rho bu} \tag{1.6}$$

Total drag $\mathbf{D}$ can be expressed in terms of induced drag $\mathbf{D}_i$ and the sum of profile and parasitic drag $\mathbf{D}_p$ as

$$\mathbf{D} = \mathbf{D}_i + \mathbf{D}_p. \tag{1.7}$$

Induced drag is related to the wing root circulation, while profile and parasitic drag are related to the airspeed over wing and the body drag coefficient. For the body drag coefficient we will continue to use $C_D \approx 0.28$ we calculated using the experimental relation from Pennycuick (1987) in equation 1.4. Continuing to follow Rayner (1991), we have a few expressions for $\mathbf{D}_i$ and $\mathbf{D}_p$ using $\hat{\mathbf{x}}$ as the direction of flight.

$$\mathbf{D}_i(\Gamma_0) = -\frac{\pi\rho\Gamma_o^2}{8}\,\hat{\mathbf{x}}, \tag{1.8}$$

As the image vortex experienced in ground effect alters the wing root circulation, the definition of induced drag in equation 1.8 is useful for assessing the influence of ground effect. We can plug in equation 1.6 to obtain an expression for induced drag as a function of airspeed over wing as

$$\mathbf{D}_i(u) = -\frac{2}{\pi\rho}\left(\frac{Mg}{bu}\right)^2\hat{\mathbf{x}}. \tag{1.9}$$

Equation 1.9 will be useful for assessing the drag experienced out of ground effect. The parasitic drag equation comes from the standard Kutta-Joukowski approach and can be written as

$$\mathbf{D}_p(u) = -\frac{\rho S C_D u^2}{2}\,\hat{\mathbf{x}}. \tag{1.10}$$

Plugging equations 1.8 and 1.10 into equation 1.7 then projecting into the flight direction gives the following expression for the magnitude of the total drag as a function of wing root circulation and airspeed over wing, written

$$D(\Gamma_0, u) = \frac{\pi\rho\Gamma_0^2}{8} + \frac{\rho S C_D u^2}{2}. \tag{1.11}$$

Plugging equations 1.9 and 1.10 into equation 1.7 then projecting into the flight direction gives the following expression for the magnitude of the total drag as a function of airspeed over wing only, written

$$D(u) = \frac{2}{\pi\rho}\left(\frac{Mg}{bu}\right)^2 + \frac{\rho S C_D u^2}{2}. \tag{1.12}$$

Minimizing the magnitude of total drag using airspeed u as the independent variable, Rayner (1991) shows that the magnitude of the minimum energy cost velocity (u_{mc}) can be expressed as

$$u_{mc} = \sqrt{\frac{2Mg}{\rho b\sqrt{\pi S C_D}}}. \tag{1.13}$$

The power output by the animal to overcome the drag force and maintain constant velocity is given by $P = \mathbf{D}\cdot\mathbf{u}$, where $\mathbf{u}$ is the velocity of airflow over the wing in absence of any external wind influence. As $\mathbf{D}$ and $\mathbf{u}$ both act in $\hat{\mathbf{x}}$, we can simply multiply the magnitudes, yielding the following general expression for the required power output out of ground effect (oge)

$$P_{oge} = uD_i + uD_p. \tag{1.14}$$

Substitution gives the following equivalent expressions for power output. In equation 1.15 we write the expression as a function of wing root circulation and velocity, while in equation 1.16 we write the expression for power output as a function of velocity only. This gives

$$P_{oge}(\Gamma_0, u) = \frac{\pi\rho u\Gamma_0^2}{8} + \frac{\rho S C_D u^3}{2}, \tag{1.15}$$

$$P_{oge}(u) = \frac{2}{\pi\rho u}\cdot\left(\frac{Mg}{b}\right)^2 + \frac{\rho S C_D u^3}{2}. \tag{1.16}$$

Plugging in the density of air and values corresponding to the brown pelican as given in table 1.1 and using the coefficient of drag from equation 1.4, we find that

$$u_{mc} = 5.7 \text{ m/s}, \quad \text{for Pelicanus Occidentalus.} \tag{1.17}$$

In assessment of $P_{oge}(u_{mc})$ for the brown pelican we see that

$$P_{oge}(u_{mc} = 5.7m/s) = 28.2\ W. \tag{1.18}$$

1.3 Flight in Ground Effect

To assess how the required power output changes in ground effect, Rayner (1991) numerically computed two ground effect interference coefficients, σ and τ. σ and τ are functions of the nondimensional height defined as $\beta \equiv 2H/b$ where H is the height above the ground and b is the wingspan. The image vortex experienced in ground effect changes the wing root circulation required to maintain flight at constant speed. The coefficient τ captures this effect, as shown by Rayner (1991) in the vertical force balance, given

$$Mg = \frac{\pi\rho b u}{4}\Gamma_0 - \frac{\pi\rho\tau}{8}\Gamma_0^2. \tag{1.19}$$

This leads to a quadratic expression for the wing root circulation as

$$\Gamma_0 = \frac{bu}{\tau} - \sqrt{\left(\frac{bu}{\tau}\right)^2 - \frac{8Mg}{\pi\rho\tau}} \tag{1.20}$$

Hainsworth (1987) found the average height of soaring flight in ground effect for a Brown Pelican to be $H_{ge} \approx 0.33m \pm 0.05m$, which yields $\beta \in (0.27, 0.36)$ with $\beta_{avg} \approx 0.31$. From the numerical results of Rayner (1991) and the observed soaring height of the brown pelican from Hainsworth (1987), we obtain values for $\Gamma_0(\beta, u_{mc})$ displayed in Table 1.1.

Rayner uses the second ground effect coefficient, σ, to relate the induced drag in and out of ground effect by the expression

$$D_{i,ge}/D_{i,oge} = 1 - \sigma. \tag{1.21}$$

It follows from substituting equation 1.21 into equation 1.15 that the required mechanical power output in ground effect, P_{ge} can be expressed as

$$P_{ge}(u) = \frac{\pi\rho u(1-\sigma)\Gamma_o^2(\beta, u)}{8} + \frac{\rho S C_D u^3}{2} \tag{1.22}$$

Plugging in values for a Pelican flying at $u_{mc} = 5.7m/s$, we obtain results displayed in table 1.2. Comparing to $P_{oge}(u_{mc}) = 28.2$ W, we see that the bird achieves a maximum of 14.2% decrease in required mechanical power output while flying at $H = 0.28$m and an average decrease in required mechanical power output of 11.0% for ground effect flight. Furthermore we see how the

Table 1.2: Ground Effect Interference Coefficients and resulting Wing Root Circulation for Pelican traveling at height $H \in H_{ge}$ and velocity u_{mc}

H	0.28	0.33	0.38
β	0.27	0.31	0.36
σ	0.40	0.35	0.32
τ	0.81	0.64	0.57
$\Gamma_o(\beta, u_{mc})$	2.52	2.46	2.44

Table 1.3: Mechanical Power Advantage for a Brown Pelican flying in Ground Effect at height $H \in H_{ge}$ and velocity u_{mc}

H	0.28	0.33	0.38
$P_{ge}(u_{mc})$	24.2	25.1	25.6
%Advantage	14.2	11.0	9.2

wing root circulation increases with lower flying height. Compared with $\Gamma_{0,oge} = 2.30$ m^2/s we see a reasonable increase for flight in ground effect. These results are displayed in table 1.3.

Chapter 2

Airflow over Near-Shoaling Waves

2.1 Introduction

As ocean waves translate, they induce airflow as a result of the no-penetration condition on a rigid boundary. Even in the case where there is no ambient wind, traveling waves move the air above them to create what is referred to as "wave-induced wind." This phenomenon has been suggested in the literature by Sullivan et al (2008), Hogstrom et al (2009), Smedman et al (2009), Soloviev and Kudryavtsev (2010), Hogstrom et al (2015), and Wu et al (2017). The upward transfer of momentum from ocean swell to the wind was experimentally verified by Grare et al. (2018). We quantitatively investigate wave-induced wind in the solitary limit of shallow water waves where pelicans have been observed to perform wave-slope soaring.

2.2 Mechanics of Near-Shoaling Waves

In order to quantify the effects of wave-induced wind, we make a few assumptions. From observation, we see that the pelicans utilize this effect in shallow, near-shoaling waves, just before they reach the breaking point. These shallow-water near-shoaling waves exhibit properties similar to the solitons described by the Korteweg-de Vries (KdV) Equation. To model near-shoaling waveforms, we will use KdV solitons. The KdV equation is valid in the limit of ($\lambda \gg h$) where λ is the wavelength and h is the local water depth. Solutions to the KdV equation then describe a phenomenon known as solitary waves, where nonlinear steepening is balanced by diffusion

resulting in a waveform which maintains constant shape as it translates. We will begin with the original KdV equation derived by Korteweg & de Vries (1895), which can be expressed as

$$\eta_t = \sqrt{gh}\,\eta_x + \frac{3}{2}\sqrt{\frac{g}{h}}\,\eta\eta_x + \frac{h^2}{2}\sqrt{gh}\left(\frac{1}{3} - \frac{\mathcal{T}}{\rho g h^2}\right)\eta_{xxx}. \tag{2.1}$$

Here we use standard notation where subscripts denote partial derivatives. η represents the displacement of the ocean surface from equilibrium. g represents the acceleration due to gravity. h represents the water depth, which we have assumed to be uniform in this analysis. This is a reasonable assumption, for as the pelican translates along the wave front, she remains over a waveform of nearly constant shape, thus in the frame of reference of the bird the water depth remains roughly constant in the idealized case. $\mathcal{T}$ represents the surface tension at the interface of seawater and air. ρ represents the density of seawater. The dimensionless group $\mathcal{T}/\rho g h^2$ is known as the Bond number, which relates surface tension to the gravitational force. Note that in Korteweg & de Vries (1895), the notation

$$\sigma \equiv h^3\left(\frac{1}{3} - \frac{\mathcal{T}}{\rho g h^2}\right), \tag{2.2}$$

was used to clean up the full dimensional KdV equation. We now plug in values to the expression for σ given in equation 2.2 for an order of magnitude estimate. In this analysis we use $\mathcal{T} \approx 0.073$ N/m for the surface tension at the interface between water and air, and $\rho \approx 1030$ for the density of seawater. Using the standard value for g of 9.8 m/s we see that

$$\begin{aligned} \sigma &= \frac{h^3}{3} - \frac{h\mathcal{T}}{\rho g}, \\ &= O(h^3) - O(h \cdot 10^{-6}). \end{aligned} \tag{2.3}$$

In the region of interest for our problem, h ranges on the order of a meter to tens of meters. Consequently, the surface tension term in σ is negligible compared with the ocean depth term. Thus we will make the approximation that

$$\sigma \approx h^3/3. \tag{2.4}$$

We will continue to use the sigma notation for consistency, and nondimensionalize the KdV equation by introducing the scaled coordinates

$$\tau \equiv \frac{1}{2}\sqrt{\frac{g}{h}}\, t, \qquad \xi \equiv \frac{x - \sqrt{gh}\, t}{\sigma^{1/3}}, \qquad u \equiv \sigma^{-1/3}\left(\frac{\eta}{2} + \frac{h}{3}\right). \tag{2.5}$$

This gives the canonical nondimensional form of the KdV as

$$u_\tau - 6uu_\xi + u_{\xi\xi\xi} = 0. \tag{2.6}$$

From Hereman (2009), we write the solution to this canonical form of the KdV as

$$u(\xi, \tau) = \frac{\Omega - 4\kappa^3}{6\kappa} + 2\kappa^2 \operatorname{sech}^2(\kappa\xi - \Omega\tau). \tag{2.7}$$

In this expression the wave number κ and angular frequency Ω are arbitrary nondimensional constants. Satisfying the boundary conditions that $\lim_{\xi\to\pm\infty} u(\xi, \tau) = 0$ gives $\Omega = 4\kappa^3$, from which we can write the nondimensional traveling wave solution

$$u(\xi, \tau) = 2\kappa^2 \operatorname{sech}^2(\kappa\xi - 4\kappa^3\tau). \tag{2.8}$$

Here $u(\xi, \tau)$ gives the scaled vertical displacement for any scaled position ξ and scaled time τ for arbitrary nondimensional wave number.

We now will replace the scaled free surface elevation (u), the characteristics (ξ) and the scaled time (τ) with their original definitions, yielding

$$\eta(x, t) = 4\sigma^{1/3}\kappa^2 \operatorname{sech}^2\left[(\kappa\sigma^{-1/3})x - \left(\frac{\kappa\sqrt{gh}}{\sigma^{1/3}} + 2\kappa^3\sqrt{\frac{g}{h}}\right) t\right]. \tag{2.9}$$

We notice that the argument of sech^2 is of the form $(x/\bar{\lambda} - t/\bar{T})$ for

$$\bar{\lambda}^{-1} \equiv \kappa\sigma^{-1/3}, \tag{2.10}$$

$$\bar{T}^{-1} \equiv \frac{\kappa\sqrt{gh}}{\sigma^{1/3}} + 2\kappa^3\sqrt{\frac{g}{h}}. \tag{2.11}$$

Here, $\bar{\lambda}$ represents half of the characteristic pulse width and $\bar{T}$ represents the solitary time-scale as shown in figure 2.1. Furthermore, we can express the coefficients on the sech^2 in terms of the

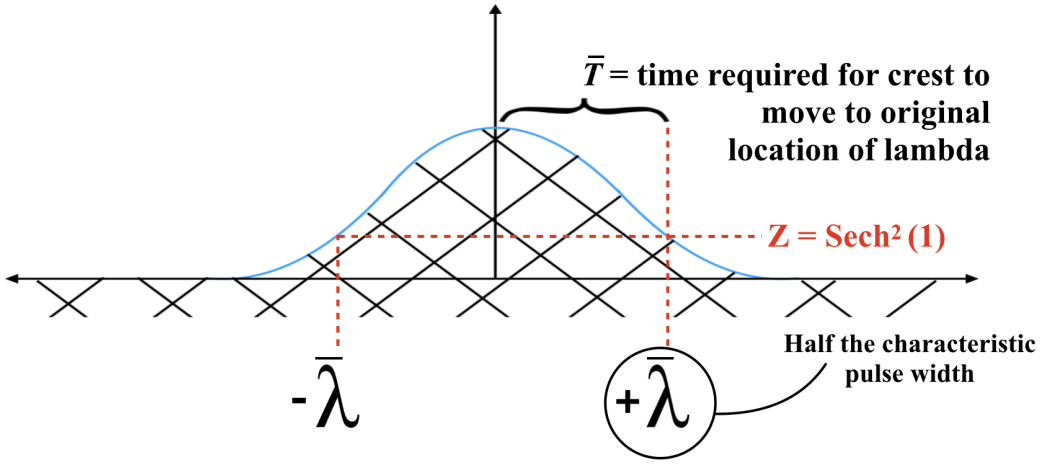

Figure 2.1: The half pulse width $\bar{\lambda}$ and the characteristic time $\bar{T}$ are displayed. $\bar{T}$ is defined as the elapsed time required for the crest to move to the previous location of $\bar{\lambda}$.

wave's amplitude as a function of κ, yielding

$$A \equiv 4\sigma^{1/3}\kappa^2. \tag{2.12}$$

As we will be using near-shore oceanographic buoy data to determine characteristics of the incoming swells, we can use the shallow water dispersion relation to write $c_0 = \sqrt{gh_0}$, where c_0 is the phase velocity at the buoy and h_0 is the ocean depth of the buoy. Note that from the buoys we can easily obtain the swell period and amplitude. The depth of oceanographic buoys are known, thus we can calculate the phase speed c_0 with the shallow water dispersion relation. From the solitary dispersion relation, it follows that the phase speed of the soliton defined as c can be expressed as $c = \bar{\lambda}/\bar{T}$.

This approximation allows us to simplify the expressions for A, $\bar{\lambda}^{-1}$, and $\bar{T}^{-1}$ as

$$A = \frac{4h\kappa^2}{3^{1/3}}, \tag{2.13}$$

$$\bar{\lambda}^{-1} = \frac{\kappa \cdot 3^{1/3}}{h}, \tag{2.14}$$

$$\bar{T}^{-1} = \kappa\frac{c_0}{h}\left[3^{1/3} + 2\kappa^2\right]. \tag{2.15}$$

We can now write the soliton's phase speed (c) in terms of the phase speed at the buoy and κ as

$$c = c_0 \left[1 + \frac{2}{3^{1/3}}\kappa^2\right]. \tag{2.16}$$

As the solitons evolve out of shallow water wave trains, we estimate the wavelength using linear shallow water wave theory with the nonlinear dispersion relation. Here we denote the period by T and wavelength by λ. This gives

$$\begin{aligned} \lambda &= T \cdot c, \\ &= T\sqrt{gh_0}\left[1 + \frac{2}{3^{1/3}}\kappa^2\right]. \end{aligned} \tag{2.17}$$

Now the last piece we need to write equation 2.7 entirely in terms of dimensional coordinates is an expression for κ in terms of known quantities. For this we will use linear wave theory, with flux (F), defined as

$$F \equiv c_{group}(x) \cdot E(x) = \text{constant}, \tag{2.18}$$

where E is the total energy, defined as

$$E = \frac{1}{16}\rho g A^2. \tag{2.19}$$

As the buoys we collect our data from are near-shore, the waves in this regime obey the shallow water dispersion relation. This gives

$$c_{group} = c_{phase} = \sqrt{g \cdot h(x)}. \tag{2.20}$$

The amplitude of the wave varies with ocean depth, so the amplitude read out by the buoy will not be the same as the amplitude in the wave-slope soaring zone. Consequently we will write $A \to A(x)$. Setting the flux at the buoy equal to the flux at some distance x inshore from the buoy, we find that

$$A(x) = A_0 \left[\frac{h_0}{h(x)}\right]^{1/4}, \tag{2.21}$$

where A_0 is the significant wave height measured by the buoy. Rearranging equation 2.13 gives an expression for κ, now that we have an expression for amplitude in terms of known quantities.

This results in

$$\kappa = \left[\frac{A(x) \cdot 3^{1/3}}{4 \cdot h(x)}\right]^{1/2}. \tag{2.22}$$

Now we can write equation 2.7 in terms of known quantities as

$$\eta(x,t) = A(x)\text{sech}^2\left[x/\bar{\lambda} - t/\bar{T}\right]. \tag{2.23}$$

Using the derived definition of κ, phase velocity and wavelength can be expressed in terms of local amplitude and local ocean depth as

$$\begin{aligned} c &= \sqrt{gh_0}\left[1 + \frac{A(x)}{2h(x)}\right], \\ \lambda &= T \cdot \sqrt{gh_0}\left[1 + \frac{A(x)}{2h(x)}\right]. \end{aligned} \tag{2.24}$$

For reasonable ocean depth, the second term in brackets acts as a correction term for soliton behavior. As the local ocean depth becomes small however, the correction term grows and our theory no longer holds, for at this point the nonlinear steepening overpowers dispersive effects and the soliton model is no longer valid.

As the expression for $A(x)$ contains $h(x)$, for a simplified model we will consider bathymetry with a linear slope. For instance, the Scripps nearshore buoy is located approximately 0.6 miles offshore from the Scripps Pier. Sitting in water depth of $h_0 = 38.7$ m, this results in a slope of roughly 0.04. We can then write an expression for $h(x)$ as $h(x) = 38.7 - 0.04x$. This sort of equation could be adapted for any nearshore buoy to get a zero order approximation of the spatial dependence of the amplitude. Generally this becomes

$$h(x) = h_0 - \alpha x, \tag{2.25}$$

where h_0 is the depth of water at the buoy location, α is the slope, and x is the distance from the buoy towards shore. Now, if we are provided with some oceanographic buoy data, we have a full mathematical description for the conditions where wave-slope soaring can be employed.

2.3 Boundary Layer Effects

In order to accurately assess the wave-induced wind, it is critical to gain an understanding the boundary layer effects corresponding to ocean waves. Full treatment of the boundary layer over the ocean is in general, complex. Immediately above the ocean is the viscous boundary layer, which exists within the atmospheric boundary layer (ABL). Following the review by Garratt (1994) it is clear from the typical length scales of the ABL that the entire wave-slope soaring process will take place within the ABL. We will be assessing the wave-induced wind in the case of a still atmosphere. Accordingly, the upper edge of the atmospheric boundary layer will have no effect on the solution.

In a theoretical study by Banner and Melville (1976) it is argued that the viscous boundary layer will not separate if a waveform maintains a smooth and steady shape. They propose that only upon the onset of shoaling will the boundary layer proceed to separate. In this case, the boundary layer will separate at the point of the crest where the shoaling process begins, resulting in a connected boundary layer on the front side of the wave and a detached boundary layer in the rear. This theory is confirmed by Reul et al (1999), who show that for shoaling waves, the viscous boundary layer separates when a discontinuity in slope develops at the crest. Their work is in agreement with the conjecture of Banner and Melville (1976) that the separated boundary layer reattaches at the front slope of the following wave.

As wave-slope soaring takes place on the front (shore side) of ocean swells before shoaling occurs, it is reasonable to assume a viscosity-dominated, well attached boundary layer over the zone of interest. As the wave-slope soaring bird will in general not fly in the region behind the near-shoaling wave where boundary layer separation may occur, it is reasonable to ignore any possible separation effects. We now focus on the viscous boundary layer immediately above the front side of a solitary wave. We estimate a length scale of this boundary layer in the limit of wave-induced wind through analysis of the Reynolds and Mach numbers.

For the evaluation of these dimensionless parameters corresponding to the wave-induced wind, we use characteristic velocity scale $u_c = v$ and characteristic length scale $l_c = \lambda$. Here v is the velocity of the wave and λ is the wavelength. Plugging in some typical values for ocean waves we see that $\mathrm{Re} = O(10^7)$, and $\mathrm{Ma} \ll 0.2$. With such a small Mach number we will continue to assume that the compressible effects are negligible. Thus, our prior assumption that ρ is constant throughout the flow remains accurate in the description of wave-induced wind. As the Reynolds

number is large (Re $\gg 1000$) it is evident that a turbulent boundary layer must exist. Inside the boundary layer, viscous forces dominate. We now introduce a viscous length scale δ which corresponds to the length scale of this turbulent boundary layer. Within the boundary layer, the viscous term and the convective term of the Navier-Stokes equations must balance, which gives an order of magnitude estimate for the length scale of the boundary layer. To give an upper bound on δ, we plug in characteristic values corresponding to flow over large, fast waves, which gives

$$\begin{aligned} O(\mu\nabla^2\mathbf{u}) &= O(\rho(\mathbf{u}\cdot\nabla)\mathbf{u}), \\ \mu\frac{u_c}{\delta^2} &= \rho\frac{u_c^2}{l_c}, \\ \delta &\leq \sqrt{\frac{\mu l_c}{\rho u_c}}, \\ \implies \quad \delta &\leq O(10^{-2}) \text{ m}. \end{aligned} \tag{2.26}$$

In typical, smaller swells where wave-slope soaring is more commonly observed, the turbulent boundary layer has a calculated length scale of $O(10^{-3})$ m. These calculated length scales are in reasonable agreement with numerical simulations by Yang et al (2018) and theoretical estimates of Reul et al (1999). Due to the length scale of a pelican and the fact that it cannot risk crashing, the bird flies on height scales of $O(10^{-1})$ while wave-slope soaring. As the bird's soaring height is much greater than the thickness of the turbulent boundary layer, we will neglect the boundary layer in calculations. Outside of the boundary layer, viscous effects are negligible and therefore we can assume inviscid flow in the regime relevant to wave-slope soaring.

2.4 Potential Flow over Solitary Waves

At this point, the wave-induced wind that we aim to describe is reasonably assumed to be inviscid, irrotational, and incompressible within our region of interest. As a result, it is appropriate to approximate the flow induced on the front side of passing solitary waves using potential flow theory. The goal is to model potential flow over the soliton

$$\eta = A\,\mathrm{sech}^2(kx), \tag{2.27}$$

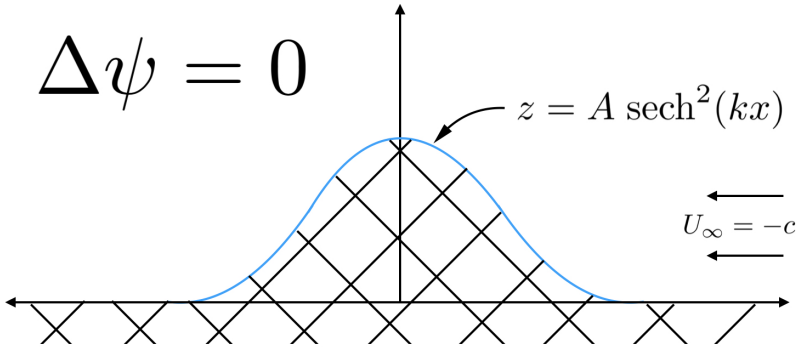

Figure 2.2: Schematic of the potential flow problem setup in the $x - z$ plane.

moving at a speed c. Here, k is defined as $\kappa\sigma^{-1/3}$ and is meant to represent a wavenumber. Although the solitons themselves are not periodic, as they evolve from periodic shallow water wave trains, this is a reasonable approximation. We first boost to a frame of reference moving with the soliton such that $U_\infty = -c$, as shown in figure 2.2. As we are assuming potential flow conditions, the system is governed by the Laplacian of the stream function

$$\Delta\psi = 0. \tag{2.28}$$

Again, due to potential flow conditions, rather than no slip we impose the no penetration boundary condition

$$[\mathbf{u} \cdot \hat{\mathbf{n}} = 0]_{z=A\ \mathrm{sech}^2(kx)}\,. \tag{2.29}$$

This is problematic for obtaining an analytical solution, as we have to solve Laplace's equation with troublesome geometry. We can get around this issue by expanding the boundary condition. First, we will nondimensionalize by defining

$$\zeta = kz, \xi = kx. \tag{2.30}$$

We will continue to use the approximation written in equation 2.12 that

$$\sigma \approx h^3/3. \tag{2.31}$$

From equations 2.8, 2.10, and 2.12 we see that

$$Ak = \frac{4}{3}(kh)^3. \tag{2.32}$$

As the soliton was derived in the limit of $\lambda \gg h$, it follows that $kh \ll 1$. We will define another nondimensional coordinate $\epsilon \equiv Ak$ such that $\epsilon = \frac{4}{3}(kh)^3 \ll 1$. Thus we can express the boundary in terms of nondimensional coordinates as

$$\zeta = \epsilon \, \mathrm{sech}^2(\xi). \tag{2.33}$$

Now, because ϵ is small, in the scaled geometry to first approximation we simply have to solve Laplace's equation in the upper half plane. By the definition of the stream function, we have

$$u = \frac{\partial \psi}{\partial \zeta}, \tag{2.34}$$

$$w = -\frac{\partial \psi}{\partial \xi}. \tag{2.35}$$

In terms of the stream function, the no penetration boundary condition (equation 2.29) can be expressed as

$$\psi = \text{constant everywhere on sea surface.} \tag{2.36}$$

Integrating equation 2.34, using the condition that as $\xi \to \pm \infty$, $\psi \to -c\,\zeta$, and using equation 2.36 gives the condition that

$$\psi = 0 \text{ everywhere on sea surface.} \tag{2.37}$$

We can equivalently express equation 2.37 as

$$\psi(\xi, \epsilon \, \mathrm{sech}^2 \xi) = 0. \tag{2.38}$$

Now, as $\epsilon \ll 1$ we will Taylor expand equation 2.38. This gives

$$\psi(\xi, 0) + \epsilon \, \mathrm{sech}^2(\xi)\psi_\zeta(\xi, 0) + \frac{1}{2}\,\epsilon^2 \mathrm{sech}^2(\xi)\psi_{\zeta\zeta}(\xi, 0) + O(\epsilon^3) = 0, \tag{2.39}$$

where subscripts denote partial derivatives. We now expand ψ in a regular expansion, yielding

$$\psi = \psi_0 + \epsilon\ \psi_1 + \epsilon^2\ \psi_2 + O(\epsilon^3), \tag{2.40}$$

where for all ψ_n with $n \in [0, \infty)$, $\Delta\psi_n = 0$. Looking at $O(\epsilon^0)$ gives $\Delta\psi_0 = 0$. Integration yields

$$\psi_0 = -c\ \zeta, \qquad \Longrightarrow \qquad \psi = -c\ \zeta + \epsilon\ \psi_1 + \epsilon^2\ \psi_2 + O(\epsilon^3). \tag{2.41}$$

Now plugging into the Taylor expanded, scaled boundary condition we obtain

$$[\epsilon\ \psi_1(\xi,0) + \epsilon^2\ \psi_2(\xi,0) + O(\epsilon^3)] + \epsilon\ \mathrm{sech}^2(\xi)[-c + \epsilon\ \psi_{1,\zeta}(\xi,0) + O(\epsilon^2)] + \frac{1}{2}\epsilon^2 \mathrm{sech}^2(\xi)[0] + O(\epsilon^3) = 0. \tag{2.42}$$

Looking at $O(\epsilon^1)$ gives

$$\psi_1(\xi,0) = c\ \mathrm{sech}^2(\xi). \tag{2.43}$$

Looking at $O(\epsilon^2)$ gives

$$\psi_2(\xi,0) + \mathrm{sech}^2(\xi)\psi_{1,\zeta}(\xi,0) + \mathrm{sech}^2(\xi)\psi_{1,\zeta}(\xi,0) = 0. \tag{2.44}$$

Using the Green's function for Laplace in 2D with the Dirichlet boundary condition in equation 2.43, we obtain an expression for $\psi_1(\xi,\zeta)$ as

$$\psi_1(\xi,\zeta) = \frac{c}{\pi}\int_{-\infty}^{\infty} \frac{\zeta\ \mathrm{sech}^2(\bar{\xi})}{(\xi-\bar{\xi})^2 + \zeta^2}\ d\bar{\xi}, \tag{2.45}$$

where $\bar{\xi}$ is the variable of integration. This is a near-singular integral with no analytical solution. To cope with this issue we will divide the domain of integration at the singularity where $\bar{\xi} = \xi$. Using this tactic and equation 2.41, we obtain a full expression for ψ as

$$\psi = -c\zeta + Ak\frac{c}{\pi}\int_0^{\infty} \frac{\zeta}{\xi'^2 + \zeta^2}\left[\mathrm{sech}^2(\xi-\xi') + \mathrm{sech}^2(\xi+\xi')\right] d\xi' + O(\epsilon^2), \tag{2.46}$$

where ξ' is our new variable of integration. This expression can now be evaluated numerically if values of ξ and ζ are specified. Using equation 2.34, we can carry out the differentiation to obtain an integral expression for the horizontal flow speed u in the frame of reference moving

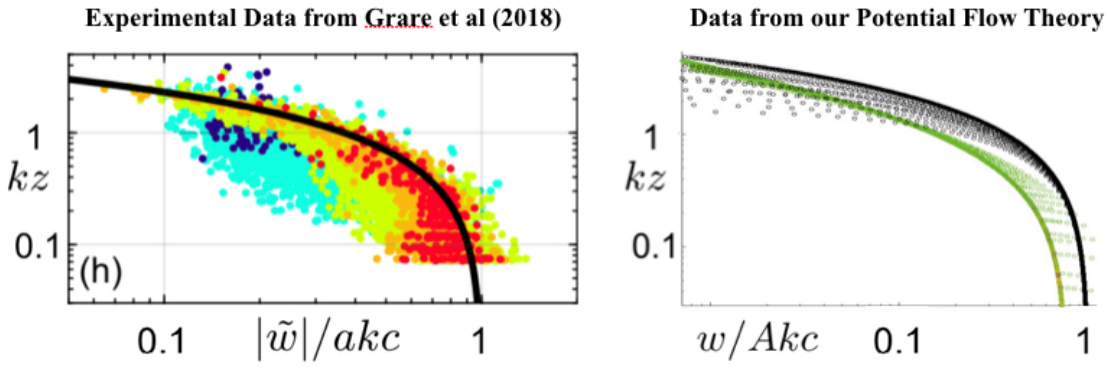

Figure 2.3: Wave-induced wind scaled with surface orbital velocity is shown on the x-axis and scaled height is shown on the y-axis in a log-log plot. The black line represents the exponential dependence (e^{-kz}) predicted by Grare et al (2018). The green dots show our predicted values of scaled flow velocity.

with the wave to the order of ϵ in terms of scaled coordinates as

$$u = -c + \frac{Akc}{\pi} \int_0^\infty \frac{\xi'^2 - \zeta^2}{(\xi'^2 + \zeta^2)^2} \left[\text{sech}^2(\xi - \xi') + \text{sech}^2(\xi + \xi')\right] \, d\xi', \tag{2.47}$$

where we have substituted the definition of ϵ ($\epsilon \equiv Ak$) back into the expression. Similarly, we can use equation 2.35 to write an integral expression for the vertical flow speed w to the order of ϵ in terms of scaled coordinates as

$$w = \frac{2Akc}{\pi} \int_0^\infty \frac{\zeta}{\xi'^2 + \zeta^2} \left[\text{sech}^2(\xi - \xi')\tanh(\xi - \xi') + \text{sech}^2(\xi + \xi')\tanh(\xi + \xi')\right] \, d\xi'. \tag{2.48}$$

As a verification of our theory, we consider waves of amplitude varying from 0.5 to 2.0 meters and period varying from 5 to 20 seconds. To compare with experimental data from Grare et al (2018), we nondimensionalize wave-induced wind with the orbital velocity at the ocean surface (Akc), and use the previously defined nondimensional vertical height $\zeta = kz$. Plotting the scaled wave-induced wind on the x-axis and scaled height on the y-axis in a log-log plot, we see reasonable agreement with experimental data from Grare et al (2018) in figure 2.3.

We now select values of x and z where we are interested in obtaining the flow velocity for wave-induced wind created by a passing soliton of given amplitude and period, then substitute into equations 2.47 and 2.48 to obtain the horizontal and vertical components of the wave-induced wind in the boosted frame, representing the flow experienced in the bird's frame of reference.

Chapter 3

Wave-Slope Soaring Flight

3.1 Introduction

In Wave-Slope Soaring, a few things occur that further improve the efficiency of the pelican's flight. First, by positioning itself on a sloping surface, the pelican is able to bring one wingtip significantly closer to the water. This allows the bird to significantly decrease its ratio of H/b over the wing semi-span, thereby improving its efficiency of flight. Second, the wave induced wind discussed in chapter two results in an incoming flow at an angle. As the bird maintains level flight through the wave induced wind, circulation over the wing is increased. This helps to satisfy the previous requirement that Γ_0 increases as H decreases. Furthermore, the inherent increase of circulation eliminates the wing supination, or manual increase in angle of attack, that is required for standard ground effect flight, consequently decreasing drag. In wave-slope soaring flight, the bird flies through a zone where the air is constantly rising, producing a similar effect to that of thermal soaring by raptors. Collectively, these factors help the pelican to save energy in flight. We will quantitatively discuss these phenomena in this chapter.

3.2 Coordinate System for Wave-Slope Soaring

We will define coordinates such that $\hat{\mathbf{x}}$ is in the direction of wave propagation, $\hat{\mathbf{y}}$ is parallel to the wave front, and $\hat{\mathbf{z}}$ is in the vertical direction. This enables us to make a few observations and assumptions. First we note that in order to gain benefit from the wave for extended periods

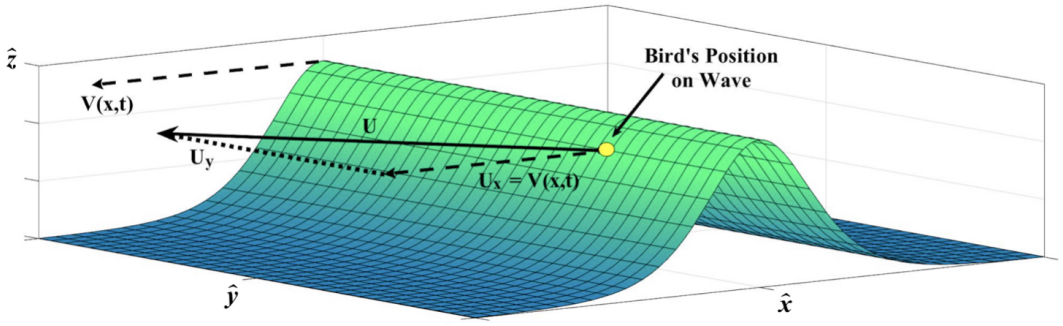

Figure 3.1: Coordinate system for the trajectories of a pelican in wave-slope soaring on a solitary wave

of time, the bird must translate in $\hat{\mathbf{x}}$ such that its velocity in the direction of wave propagation (U_x) will match the phase velocity of the wave, $V(x,t)$. As stated above, we assume that the bird translates in $\hat{\mathbf{y}}$ such that the slope of the waveform underneath of it remains constant. This results in soaring over a waveform that will remain constant in time, in the pelican's frame of reference. We also assume that in wave-slope soaring, the bird finds the optimum location in $\hat{\mathbf{z}}$ and remains at this location. All of these assumptions enable us to perform analyses wherein the slope of the wave under the bird will remain constant, as shown in Figure 3.1. Consequently, as the propagation and slope of the waveform are the only time-dependent features of the waveform, these assumptions allow us to ignore the system's time evolution and assume that the relevant wave-induced air flow is steady and irrotational in the bird's frame of reference. As we are studying the time independent case of solitons, the velocity of the wave is constant everywhere in space and time such that $V(x,t) = c$. Using the formalism developed in chapter 2, given an arbitrary swell with known period and amplitude we can determine c.

Now as the waves are propagating towards the shore and eventually shoaling, this idealized process we have described clearly cannot go on forever. From observing pelicans practicing wave-slope soaring, one can see that these assumptions are reasonable over timescales of 10-20 seconds. After 10-20 seconds the entire wave front moves beyond the solitary limit into a shoaling situation. At this point when the birds reach the shoaling section of the wave, they gain considerable altitude without flapping before soaring down to the next shore-bound wave and repeating the process. The analysis of benefits from the shoaling section are omitted in this paper. Hence, we will be considering the ideal case within this 10-20 second time frame where

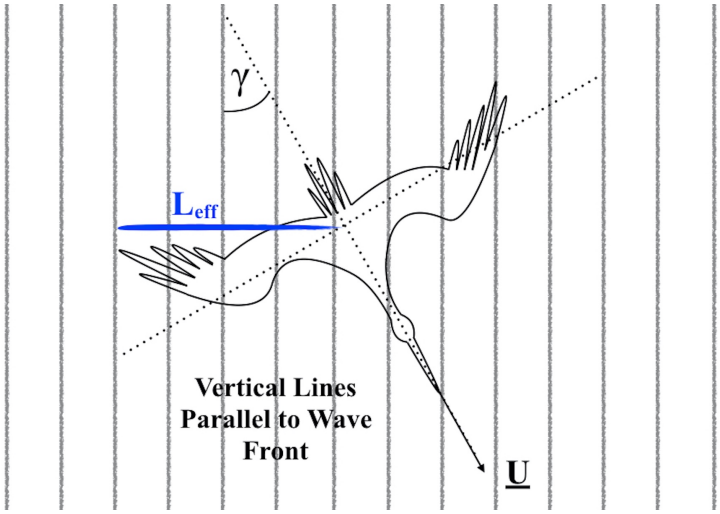

Figure 3.2: Coordinate System defining L_{eff} which relates the position of the pelican's center of mass to the position of its wingtip

wave-slope soaring is practiced.

In calculation of the wave-slope soaring power distribution, the effective height of the pelican's center of mass as a function of its wingtip location ($H_{eff}(x_{wt})$) will be necessary. To a first approximation, we will consider the case where the bird is exactly level. From observation, this is often the case. In order to assess this we set up a coordinate system where γ is defined as the angle between the bird's trajectory and lines parallel to the wave front. The perpendicular distance from the pelican's center of mass to the line parallel to the wave front that passes through the bird's wing tip, will be referred to as the effective length (L_{eff}). This coordinate system is shown in Figure 3.2. This setup, along with a simple Pythagorean argument gives us the following relations which can be combined to give L_{eff} in terms of known parameters:

$$L_{eff} = \frac{b}{2}\,\frac{\sqrt{\mathbf{U}^2 - U_x^2}}{U}. \tag{3.1}$$

As the pelican must match U_x to the wave's phase velociity c in order to utilize beneficial effects from the wave, and she will strive to set $U = u_{mc}$. Thus we can further reduce the equation for L_{eff} in the case of ideal wave-slope soaring. Here, ideal is meant to imply that the bird is able to set $U = u_{mc}$. This gives

$$L_{eff} = \frac{b}{2}\,\frac{\sqrt{u_{mc}^2 - c^2}}{u_{mc}}. \tag{3.2}$$

From figure 3.3 we see that H_{eff} and $H(x)$ can both be described in terms of x_{wt} in the

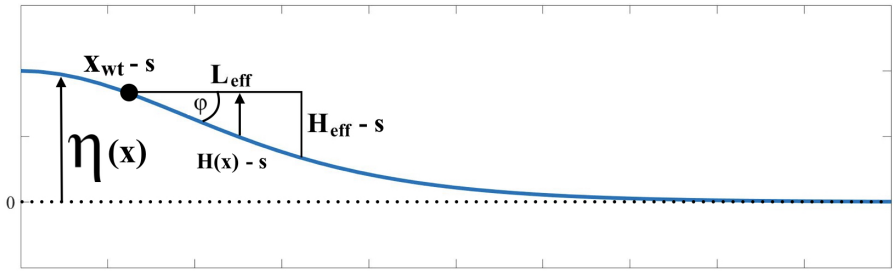

Figure 3.3: Profile view of a solitary wave. Geometric definitions of variables $\eta(x)$, L_{eff}, H_{eff}, $H(x)$, x_{wt}, and ϕ are displayed

time-independent, steady case as

$$H(x) = [\eta(x_{wt}) - \eta(x)] + s. \tag{3.3}$$

$$\begin{aligned} H_{eff} &= [\eta(x_{wt}) - \eta(x_{wt} + L_{eff})] + s, \\ &= \left[\eta(x_{wt}) - \eta\left(x_{wt} + \frac{b}{2} \cdot \frac{\sqrt{u_{mc}^2 - c^2}}{u_{mc}}\right)\right] + s, \end{aligned} \tag{3.4}$$

where s is the safety margin employed by the pelican to avoid crashing. To maximize use of the updrafts created by waves, the bird will position itself over the zone of the wave where the vertical component of the wave induced wind is the greatest. It follows from chapter 2 that this location is where the slope of the wave is the most negative. Denoting the slope of the wave as m_{wave} we obtain an equation for x_{wt} as

$$\begin{aligned} x_{wt} &= \text{Min}\,(m_{wave}) - L_{eff}, \\ x_{wt} &= \text{Min}\left(\frac{\partial \eta}{\partial x}\right) - L_{eff}, \\ x_{wt} &= \text{Min}\left(-2Ak\,\tanh(kx)\text{sech}^2(kx)\right) - L_{eff}. \end{aligned} \tag{3.5}$$

3.3 Analysis and Results

We will study this idealized case now, with the approximation that the bird flies exactly level with horizontal and positions itself exactly over the inflection zone of the wave. We will begin from first principles and consider the mechanical energy balance of the system following Taylor et al (2016), assuming that the energy lost to the sound of flight is negligible. The total energy

of the system is given as

$$E = \frac{1}{2} M \mathbf{u}_{bird} \cdot \mathbf{u}_{bird} + M\mathbf{g} \cdot \mathbf{x}, \tag{3.6}$$

where $\mathbf{x}$ is the bird's inertial position and $\mathbf{u}_{bird}$ is the velocity of the airflow over the bird's wings. As we are interested in the required power output by the bird, we differentiate with respect to time. This gives

$$\frac{dE}{dt} = M\mathbf{u}_{bird} \cdot \frac{d\mathbf{u}_{bird}}{dt} + M\mathbf{g} \cdot \frac{d\mathbf{x}}{dt}. \tag{3.7}$$

The rate of change of the bird's inertial position is given by the vector sum of the bird's velocity relative to the air and the air's velocity relative to the ground. Formally, we can express this as

$$\frac{d\mathbf{x}}{dt} = \mathbf{u}_{bird} + \mathbf{u}_{wind}. \tag{3.8}$$

Taking another time derivative and rearranging gives

$$\frac{d\mathbf{u}_{bird}}{dt} = \frac{d^2\mathbf{x}}{dt^2} - \frac{d\mathbf{u}_{wind}}{dt}. \tag{3.9}$$

in the case we are considering of steady, constant altitude wave-slope soaring on a soliton with no ambient wind, the resulting wave-induced wind is steady. Accordingly, $d\mathbf{u}_{wind}/dt = 0$. Plugging everything back into equation 3.7 we have

$$\frac{dE}{dt} = \left[M\frac{d\mathbf{u}_{bird}}{dt} + M\mathbf{g} \right] \cdot \mathbf{u}_{bird} + M\mathbf{g} \cdot \mathbf{u}_{wind} - M\mathbf{u}_{bird} \cdot \frac{d\mathbf{u}_{wind}}{dt}. \tag{3.10}$$

As the term $\frac{d\mathbf{u}_{bird}}{dt}$ is always negative in the case with no external energy input as a result of drag, we may take the absolute value and tack on a negative sign. Evaluating the dot products, we obtain

$$\frac{dE}{dt} = Mgw_{wind} - M\left|\frac{d\mathbf{u}_{bird}}{dt}\right| \cdot \mathbf{u}_{bird}. \tag{3.11}$$

The first term on the right hand side corresponds to the potential energy harvesting benefit resulting from positioning over the updraft induced by the wave, while the second term corresponds to the loss due to drag. The difference, $\frac{dE}{dt}$, corresponds to the required mechanical power output if the bird is to maintain flight at constant velocity and altitude. For the analysis of the power associated with drag forces that the bird must overcome, we will again follow the lifting line theory of flight in ground effect with a fixed wing detailed by Rayner (1991) that we

Table 3.1: Relevant values for wave-slope soaring over a soliton generated from wind swell at $s = 0.2$ m.

T	A	c	u_1	u_2	w_1	w_2	H_1	H_2
10 s	1 m	5.24 m/s	5.47 m/s	5.44 m/s	0.40 m/s	0.39 m/s	0.22 m	0.26 m

discussed in chapter 1. For an initial approximation, we will consider the effect of each wing separately. From equation 3.4, the effective height of the wing closer to the crest denoted H_1 is given as

$$H_1 = \eta(x_{wt}) - \eta\left(x_{wt} + \frac{b}{4} \cdot \frac{\sqrt{u_{mc}^2 - c^2}}{u_{mc}}\right) + s. \tag{3.12}$$

Analogously, the height of the wing further from the crest can be written as

$$H_2 = \eta(x_{wt}) - \eta\left(x_{wt} + \frac{3b}{4} \cdot \frac{\sqrt{u_{mc}^2 - c^2}}{u_{mc}}\right) + s. \tag{3.13}$$

The scaled heights β_1 and β_2 are then simply given by

$$\beta_i = \frac{2H_i}{b}, \tag{3.14}$$

for $i = 1, 2$. The safety margin s is a function of the slope of the wave and the shape of the bird employing wave-slope soaring. For the brown pelican the lowest point of the bird's airfoil is its belly. For a pelican with a wingspan of 2.1m, using photo scaling we find that the belly extends roughly ten centimeters below the wing line. We then assume that for a margin of safety, the bird will keep the low point of its belly at least ten centimeters above the surface of the ocean throughout the wave slope soaring process. We will accordingly take s to be roughly 0.2m in order to account for the belly and airspace beneath. Now we have all of the pieces together to analyze the power benefit of wave slope soaring. In assessment of typical wind swell conditions, we will assume a dominant swell period of ten seconds with an amplitude of one meter. From chapter 2, we obtain values of the phase velocity, horizontal and vertical flow speeds in the bird's frame of reference at the height of the pelican for each wing's central location. These are denoted c, u_i, and w_i respectively for $i = 1, 2$ according to the convention in equation 3.14. From equations 3.12 and 3.13, we obtain H_1 and H_2. This data is displayed in table 3.1. From the values of H_1 and H_2, we obtain values for β_1 and β_2 as 0.21 and 0.25, respectively.

With the airflow impinging at an angle determined by the ratio of vertical to horizontal

Table 3.2: Ground-effect interference coefficients and wing root circulation for wave-slope soaring.

s	0.29	0.20	0.11
β	0.31	0.23	0.14
σ	0.35	0.46	0.54
τ	0.64	0.92	1.16
Γ_0	2.46	2.55	2.64
u	5.49	5.46	5.44
w	0.38	0.40	0.41

flow velocities, circulation over the wing is consequently increased. As the wavelength is large compared to the wingspan of the bird and the wave-induced wind varies little over the wingspan of the bird, we take the average from contributions to each wing in calculation of the ground effect interference coefficients and wing root circulation. To form an upper bound on the benefits of wave-slope soaring, we allow the safety margin s to drop to 0.11m. This is an unrealistic case as it only allows for 1cm of space before the pelican's belly hits the water, but it will provide the maximum benefit. In this case, β drops to 0.14. For a lower bound/control parameter, we set $s = 0.29$ such that the average height of the bird above the wave equals the average height of brown pelican ground effect flight as observed by Hainsworth (1988). In this case, β remains unchanged from the studies in chapter 1. This data along with the average components of the wave induced wind in a frame of reference moving with the wave is displayed in table 3.2 for each value of s.

In the case with a safety margin of 0.29 m, the drag forces require 25.1W of power to maintain flight. The benefit from the updraft at this altitude is 9.87W, yielding a required power output of 15.23W from our pelican. At a safety margin of 0.2m the drag forces require 23.4W of power to maintain flight. At this height, the benefit from the updraft (Mgw) amounts to 10.39W, resulting in a required power output of 13.01W from the bird. In the extreme case where we let the safety margin drop to 0.11m, power output required for steady flight drops to 22.6W. Benefit from the updraft has a meager uptick to 10.65W. This results in a required power output of 11.95W from the bird. These results are compared with the out-of-ground-effect and standard-ground-effect power distributions in table 3.3. A breakdown of the sources of power is detailed in table 3.4.

Table 3.3: Mechanical power output required from bird and percent advantage for ground effect and wave-slope soaring as compared to standard flight out of ground effect.

Mechanical Power Output	P_{oge}	P_{ge}^{max}	P_{ge}^{avg}	P_{ge}^{min}	$P_{ws}^{control}$	P_{ws}^{avg}	P_{ws}^{min}
Value	28.2	25.6	25.1	24.2	15.23	13.01	11.95
% Advantage Compared to OGE	0	9.2	11.0	14.2	46.0	53.9	57.6

Table 3.4: Breakdown of the various sources of power benefit.

	OGE	GE, WS	GE, WS	GE, WS
β	∞	0.31	0.23	0.14
Total Power Required	28.2	25.1	23.4	22.6
Power Reduction from Ground Effect	0	3.1	4.8	5.6
Power Reduction from W-S Soaring	0	9.87	10.39	10.65
Power Output Required from Bird	28.2	15.23	13.01	11.95

Chapter 4

Discussion

4.1 Setup and Assumptions

We theoretically assess the energy savings associated with wave-slope soaring flight. In particular, we study the brown pelican practicing wave-slope soaring over near-shoaling coastal waves. We assume inviscid, incompressible, constant density flow throughout the regime where wave-slope soaring is employed. We assume a small angle of attack, such that flow separation over the pelican's wings does not occur. To model the brown pelican, we use elliptic wing-loading theory. An experimental value for the brown pelican's coefficient of lift determined by Pennycuick (1982) is used, while the coefficient of lift is derived based on theory by Pennycuick et al (1987). Average pelican dimensions determined by Pennycuick (1982) are used throughout the paper. We find the Reynold's number of the flow over the pelican's wings to be 150,000.

4.2 Flight out of Ground Effect

We analyze the steady, constant altitude flight of a pelican in still air, out of ground effect as a control. We use the Kutta˙Joukowski theorem to assess lift and wing-root circulation as a function of flight speed. Total drag is decomposed into induced, profile, and parasitic drag. Following Rayner (1991), we determine expressions for the various elements of drag. Minimizing the total drag using the speed of the air flow over wings as the independent variable gives an expression for the minimum cost velocity in terms of known parameters. This speed, denoted

u_{mc} is found to be 5.7 m/s for the brown pelican. We then find the required power output for a brown pelican to remain in steady, constant altitude flight to by 28.2 Watts.

4.3 Flight in Ground Effect

We use the ground effect interference coefficients numerically derived by Rayner (1991) to assess how the required power output changes in ground effect. We find that in ground effect, the wing root circulation increases, the minimum cost velocity remains constant, and the required power output decreases. Based on data detailing the typical height of pelican flight in ground effect from Hainsworth (1987), we find an average of an 11% decrease in power output for a pelican utilizing ground effect. The range of benefit was found to be 9.2% benefit on the upper end of ground effect flight height and 14.2% benefit on the lower end of the range of flight heights given by Hainsworth (1987).

4.4 Airflow over Near-Shoaling Waves

The airflow induced by a passing wave, or the "wave-induced wind" is theoretically analyzed for near-shoaling shallow water solitary waves. These waves are assumed to be well described by the KdV equation. We follow Korteweg & De Vries (1895) and Hereman (2009) to derive a dimensional solution to the KdV equation for shallow water waves. We ignore the effects of surface tension as we are dealing with large gravitational ocean surface waves to develop a framework wherein when supplied with buoy data of the period and amplitude of an incoming swell, the variation in amplitude, phase velocity, and wavelength as the swell approaches shore are produced.

In deriving the wave-induced wind, we assume negligible boundary layer effects within the regime where wave-slope soaring will be employed. Thus, with our previous assumptions, we are able to use potential flow theory to describe the wave-induced wind. We nondimensionalize with wavenumber in order to expand the boundary condition such that our problem reduces to solving Laplace's equation in the upper half plane. Using a regular expansion of the Stokes stream function and the Green's function for Laplace in 2D with Dirichlet boundary conditions, we obtain integral expressions for the horizontal and vertical components of the wave-induced wind in a frame of reference moving with the wave. We split the range of the integral expressions

in order to eliminate the near-singularity, resulting in numerically soluble expressions. The theory results in expressions wherein provided with the buoy data of amplitude and period of an incoming swell, horizontal and vertical components of the wave induced wind in a frame of reference moving with the wave are produced.

4.5 Wave-Slope Soaring Flight

Wave-slope soaring flight is analyzed over near-shoaling solitary waves on size scales corresponding to windswell, as these are the most commonly observed ocean surface waves. We assume that the pelican matches its velocity in the direction of wave propagation to match the phase velocity of the wave. This enables the bird to make use of the wave-induced wind for extended periods of time. As we are working in the solitary limit of shallow water waves, we ignore any time dependence of the system resulting in a waveform that is constant in time. We further idealize by assuming symmetry along the wave-front.

We put the bird in the picture centered at the inflection point of the waveform, such that it can maximize use of the updraft produced from a translating wave. A safety factor is set to account for efforts the bird will take to balance the necessity of avoiding a crash with the aim to maximize benefit. Initially, effects from each wing are considered independently. Upon inputting values, we find it is reasonable to average over the length of the wing as the wavelength is much greater than the projected wingspan of the bird. Wing root circulation and the ground effect interference coefficients are calculated for different safety factors under sea surface conditions with 1 meter amplitude and 10 second period. The mechanical power output is calculated and compared to the values for flight out of ground effect as well as standard ground effect flight. We find an upper bound benefit of 57.6% decrease in required mechanical power output as compared with flight out of ground effect and 52.4% benefit as compared with standard ground effect.

Even in our bounding case for minimum benefit from the wave's effects, the resulting benefit is extraordinary with 46.0% advantage as compared to flight out of ground effect. In the case with a plausible safety factor, we find 53.9% decrease in the required mechanical power output for wave-slope soaring flight. The maximum possible percent advantage we find for wave-slope soaring on standard wind swell was 57.6%. This provides a significant incentive for birds to utilize the practice. With a sufficient safety factor, this benefit in flight performance could

be enough to incentivize use of the practice by manmade UAVs. It is possible that the aircraft could be designed with the use of wave-slope soaring in mind, resulting in even larger percent advantages. The theory in this work present sufficient evidence that the use of wave-slope soaring by UAVs should be considered, provided that the margin of safety is sufficient to avoid crashing.

4.6 Further Research

The primary limitation of the theory presented in this work is the restriction to solitary waves. In reality, when observing pelicans employing wave-slope soaring, it is common for them to soar well beyond the solitary limit. They often will maintain wave-slope soaring all the way to the point of shoaling, where the updraft becomes so strong it sends them several meters in the air without flapping. When all the conditions align, this allows the birds to soar to the next incoming wave and repeat the process, all without flapping. With these observations it is clear that the benefit from the shoaling sections of incoming ocean waves must be considered to fill out the theory.

In the period of time beyond solitary limit where nonlinear steepening is increasing, this also increases the wave-induced wind. It is evident that this zone can provide significant benefit as pelicans are often observed using wave-slope soaring in this region. Furthermore, we saw that for an uptick in vertical wave-induced velocity from 0.38m/s to 0.41m/s, the power input from the wind jumped all the way from 9.87W to 10.39W. This is a significant increase for such a small change in windspeed. When waves surpass the solitary limit and move closer to shoaling, the vertical component of the wave-induced wind increases significantly. This could vastly improve the bird's efficiency of flight, perhaps to the point where the power delivered by the wind outweighs the power required by drag. In short, to fully develop this theory we need to account for the time evolution of the system. This would involve tracking the evolution of the wave form from the solitary limit all the way to the point of shoaling. It would be interesting to observe how the percent advantage changes as the wave tracks towards shoaling.

We have considered wave-slope soaring in the case where the bird is able to fly with a net velocity equal to the minimum cost velocity as derived in chapter 1. It is clear that there is significant benefit to be gained from wave-slope soaring, as shown in chapter 3. We studied the case of common wind swell as the phase velocity of wind swell is less than the minimum cost

velocity for a brown pelican, allowing the bird to perform wave-slope soaring while flying at its minimum cost velocity. Larger waves move faster, so for a pelican to soar on such a wave it will have to exceed its minimum cost velocity which will result in an increase in drag. However, if the wave is steep enough such that the vertical component of the wave induced wind is significant, the benefit from the wave could outweigh the loss from increased drag. It would be useful for this theory to study this cost-benefit relationship in greater detail, for waves that have moved beyond the solitary limit into a situation that is closer to shoaling.

Bibliography

[1] Denny, M. (2009). Dynamic soaring: aerodynamics for albatrosses. *Eur. J. Phys.* **30**, 75-84.

[2] Garratt, J.R. (1994). Review: the atmospheric boundary layer. *Earth-Sci. Rev.* **37**, 89-134.

[3] Grare, L., Lenain, L., Melville, W. K. (2018). Vertical Profiles of the Wave-Induced Airflow above Ocean Surface Waves. *J. of Phys. Oceanography* **48**, 2901-2922.

[4] Hainsworth, F Reed. (1988). Induced Drag Savings from Ground Effect and Formation Flight in Brown Pelicans. *J. exp. Biol.* **135**, 431-444.

[5] Hereman, Willy. (2009). Shallow Water Waves and Solitary Waves. *Encyclopedia of Complexity and Sys. Sci.* 8112-8125.

[6] Hogstrom, U., A. Smedman, E. Sahlee, W. M. Drennan, K. K. Kahma, H. Pettersson, and F. Zhang, (2009). The atmospheric boundary layer during swell: A field study and interpretation of the turbulent kinetic energy budget for high wave ages. *J. Atmos. Sci.* **66**, 2764–2779.

[7] Hogstrom, U., E. Sahlee, A.-S. Smedman, A. Rutgersson, E. Nilsson, K. K. Kahma, and W. M. Drennan, (2015). Surface stress over the ocean in swell-dominated conditions during moderate winds. *J. Atmos. Sci.* **72**, 4777–4795.

[8] Korteweg, D.J., de Vries, G. (1895). On the Change of Form of Long Waves Advancing in a Rectangular Canal, and on a New Type of Long Stationary Waves. *Phil. Mag.*, **39**, 422–443.

[9] Martin, David S. (2017). An Investigation of Avian Wing Tip Vortex Generation Using a Biomimetic Approach. *Master of Science Thesis: Department of Aerospace Engineering, California State Polytechnic University.* San Luis Obispo, California.

[10] Pennycuick, C. J. (1983). Thermal soaring compared in three dissimilar tropical bird species, Fregata magnificens, Pelecanus occidentalis and Coragyps atratus. *J. Exp. Biol.* **102**, 307-325.

[11] Pennycuick, C. J., Obrecht, O. O. and Fuller, M. J. (1988). Empirical estimates of body drag of large waterfowl and raptors. *J. Exp. Biol.* **135**, 253-264.

[12] Rayner, J. M. V. (1991). On the Aerodynamics of Animal Flight in Ground Effect. *Phil. Trans: Biol. Sci.* **334**, 119-128.

[13] N. Reul, H. Branger, J. P. Giovanangeli, (1999). Air flow seperation over unsteady breaking waves. *Physics of Fluids* **11**, 1959.

[14] Richardson, P. L. (2011). How do albatrosses fly around the world without flapping their wings? *Prog. Oceanogr.* **88**, 46-58.

[15] Sachs G., J. Traugott, A. P. Nesterova, F. Bonadonna. (2013). Experimental verification of dynamic soaring in albatrosses. *J. Exp. Biol.* **216**, 4222-4232.

[16] Smedman, A., U. Hogstrom, E. Sahlée, W. M. Drennan, K. K. Kahma, H. Pettersson, and F. Zhang, (2009). Observational study of marine atmospheric boundary layer characteristics during swell. *J. Atmos. Sci.* **66**, 2747–2763.

[17] Soloviev, Y. P., and V. N. Kudryavtsev, (2010). Wind-speed undulations over swell: Field experiment and interpretation. *Bound.-Layer Meteor.* **136**, 341–363.

[18] Sullivan, P. P., J. B. Edson, T. Hristov, and J. C. McWilliams, (2008). Large-eddy simulations and observations of atmospheric marine boundary layers above nonequilibrium surface waves. *J. Atmos. Sci.* **65**, 1225–1245.

[19] Taylor, G. K., K. V. Reynolds, A. L. R. Thomas (2016) Soaring energetics and glide performance in a moving atmosphere. *Philos. Trans. R. Soc. Lond. B. Biol. Sci.* **371** 1704.

[20] Wilson, J. A. (1975). Sweeping flight and soaring by albatrosses. *Nature* **257**, 307-308.

[21] Wu, L., A. Rutgersson, and E. Nilsson, (2017). Atmospheric boundary layer turbulence closure scheme for wind-following swell conditions. *J. Atmos. Sci.* **74**, 2363–2382.

[22] Z. Yang, B. Deng, L. Shen, (2018). Direct numerical simulation of wind turbulence over breaking waves. *J. Fluid Mech.* **850**, 120-155.